International Journal of Heat and Mass Transfer 116 (2018) 1370–1378

Contents lists available at ScienceDirect

International Journal of Heat and Mass Transfer

journal homepage: www.elsevier.com/locate/ijhmt

Design and performance evaluation of a multilayer fixed-bed binder-free desiccant dehumidifier for hybrid air-conditioning systems: Part II – Theoretical analysis

Wei-Lun Hsu [a,*], Soumyadeep Paul [b], Jubair A. Shamim [a], Kenji Kitaoka [c], Hirofumi Daiguji [a]

[a] Department of Mechanical Engineering, The University of Tokyo, Tokyo 113-8656, Japan
[b] Department of Mechanical Engineering, Indian Institute of Technology (BHU), Varanasi 221-005, India
[c] Asahi Glass Co. Ltd., Technology General Div., 1-5-1 Marunouchi, Chiyoda, Tokyo 100-8405, Japan

ARTICLE INFO

Article history:
Available online 5 October 2017

Keywords:
Air-conditioning
Adsorption
Computational fluid dynamics
Desiccant
Dehumidification

ABSTRACT

The interdependent physics involved in the transport, adsorption, and thermal phenomena within desiccant-based dehumidifiers makes the construction of theoretical models essential to investigate intrinsic mechanisms. In Part II of this series, a computational model is established that increases an understanding of transient mass and heat transfer phenomena in a multilayer fixed-bed binder-free desiccant dehumidifier (MFBDD). A two-dimensional (2D) model incorporating the principles of momentum, mass and heat conservation is constructed. A modification of Darcy's law is employed to evaluate the frictional resistance due to the presence of Micro Sphere Gel (M. S. Gel) beads in the desiccant bed. In the study, the moisture adsorption characteristics of M. S. Gel are theoretically described by employing a Linear Driving Force (LDF) model and a modified Langmuir-Sips model (based on the local relative humidity RH) owing to the unique sigmoid-shape of its adsorption isotherm at various temperature levels. The energy conservation is considered to estimate phase transition latent heat because of the moisture adsorption and heat loss to surroundings through the metal frames at different process air conditions. The validity of the model is tested by comparing the theoretical predictions with experimental observations. The results indicate that the predicted adsorbed water within the MFBDD, dehumidification capacity, temperature increase, and pressure decrease based on the simulation are in quantitative agreement with the experimental results obtained in Part I. The experimentally observed transient translocation of maximum temperature inside the M. S. Gel bed is theoretically reproduced and analyzed.

1. Introduction

In Part I [1], a multilayer fixed-bed binder-free desiccant dehumidifier (MFBDD) is designed using Micro Sphere Gel (M. S. Gel), and the results indicated that its performance exceeds that of classical desiccant rotary wheel dehumidifiers. Nevertheless, the complex nature of coupled phase transition and transport phenomena prevents the complete perception of intrinsic behaviors of dynamic humidity and temperature variations inside the system. It is challenging to precisely comprehend working mechanisms solely based on experimental observations that primarily report average output quantities with a paucity of information related to local variations.

To solve the fore-mentioned challenges, computational analysis (that is extensively applied to theoretical analysis of various desiccant dehumidification systems [2–11]) is considered as a useful tool to investigate detailed momentum, mass, and energy transfer phenomena within air-conditioning systems. For example, De Antonellis et al. [3] used a one-dimensional gas-side resistance (GSR) model to investigate the optimized conditions of desiccant wheel performance by considering the heat supplied for the regeneration process and pressure drop across the wheel. Mandegari and Pahlavanzadeh [4] developed a two-dimensional (2D) model to predict the electrical energy and thermal energy required for fan operation and regeneration, respectively. Yamaguchi and Saito [5] investigated heat and mass transfer of rotary desiccant wheels by considering Knudsen and surface diffusivity within porous desiccant walls. A thermodynamic analysis for the entropy generation expression was investigated by Giannetti et al. [9] for desiccant wheel operability. Intini et al. [10] theoretically analyzed a zeolite desiccant wheel to verify experimental measurements.

* Corresponding author.
E-mail address: wlhsu@thml.t.u-tokyo.ac.jp (W.-L. Hsu).

https://doi.org/10.1016/j.ijheatmasstransfer.2017.09.080
0017-9310/

Nomenclature

a	Langmuir-Sips parameter (kg kg^{-1})
A	simulation domain of the M. S. Gel bed (m^2)
b_1	Langmuir-Sips parameter (–)
b_2	Langmuir-Sips parameter (–)
C_p	specific heat capacity of air (J kg^{-1} K^{-1})
$C_{p,\ bed}$	specific heat capacity of the M. S. Gel bed (J kg^{-1} K^{-1})
$C_{p,\ M.\ S.Gel}$	specific heat capacity of the M. S. Gel (J kg^{-1} K^{-1})
d	M. S. Gel layer thickness (m)
d_p	diameter of the M. S. Gel particles (m)
D	diffusivity of water in air (m^2 s^{-1})
h	air flow channel size (m)
h_{ads}	latent heat of adsorption (J kg^{-1})
h_c	convective heat transfer coefficient (W m^{-2} K^{-1})
h_{loss}	heat loss coefficient (W m^{-3} K^{-1})
k	thermal conductivity of air (W m^{-2} K^{-1})
k_{ads}	LDF rate constant (s^{-1})
k_{bed}	thermal conductivity of the M. S. Gel bed (W m^{-2} K^{-1})
$k_{M.\ S.\ Gel}$	thermal conductivity of the M. S. Gel (W m^{-2} K^{-1})
K	permeability (m^2)
L	length of the M. S. Gel bed (m)
m	total adsorbed water in the MFBDD (kg)
M	adsorbed water (kg kg^{-1})
M'	adsorption rate (kg kg^{-1} s^{-1})
$\langle M' \rangle$	average adsorption rate (kg kg^{-1} s^{-1})
M_{eq}	adsorbed water at equilibrium (kg kg^{-1})
M_W	molar mass of water (kg mol^{-1})
n	Langmuir-Sips parameter (–)
$\mathbf{n}$	unit normal vector (–)
N	number of M. S. Gel beds (–)
p_{sat}	saturated partial vapor pressure (Pa)
p_v	partial vapor pressure (Pa)
P	pressure (Pa)
P_{in}	inlet pressure (Pa)
P_{out}	outlet pressure (Pa)
R	ideal gas constant (J mol^{-1} K^{-1})
t	time (s)
T	temperature (K)
$\langle T \rangle$	average temperature (K)
$\bar{T}$	flow average temperature (K)
T_0	room temperature (K)
T_{in}	inlet air temperature (K)
T_{out}	outlet air temperature (K)
$\mathbf{v}$	(Darcy) air velocity vector (m/s)
$\mathbf{v}_{local}$	local air velocity vector (m/s)
v_{in}	inlet air velocity (m/s)
v_x	x-component of air velocity (m/s)
$\langle v_x \rangle$	average x-component of air velocity (m/s)
$\langle v_x T \rangle$	average product of the x-component of air velocity and temperature (m K s^{-1})
W	width of the M. S. Gel bed (m)
X	specific humidity (kg kg^{-1})
X_{in}	inlet specific humidity (kg kg^{-1})
X_{out}	outlet specific humidity (kg kg^{-1})
α_{air}	thermal diffusivity of air (m^2 s^{-1})
α_{bed}	thermal diffusivity of the M. S. Gel bed (m^2 s^{-1})
$\alpha_{M.\ S.\ Gel}$	thermal diffusivity of the M. S. Gel (m^2 s^{-1})
ΔP	pressure drop (Pa)
Δt	time difference (s)
ΔT	temperature increase (K)
ΔX	dehumidification capacity (kg kg^{-1})
ε	porosity (–)
ϕ	sphericity (–)
φ	relative humidity (Pa Pa^{-1} (%))
μ	viscosity of air (Pa s)
ρ	density of air (kg m^{-3})
ρ_{bed}	density of the M. S. Gel bed (kg m^{-3})
$\rho_{M.\ S.Gel}$	density of the M. S. Gel (kg m^{-3})

However, these theoretical studies primarily focused on rotary wheel desiccant systems by using silica gel or zeolite as an adsorbent. Thus, an independent theoretical study for the present MFBDD is required to examine mass and heat transport behaviors during the dehumidification process. Hence, the goal of the present study involves establishing a mathematical model that reproduces experimentally observed adsorption behavior in Part I. Thus, the transient responses of physical quantities with local resolution can be revealed. This is performed to acquire a deeper understanding of the mechanisms responsible for the observed phenomena, which would enrich conceptual insights for accelerating the development of MFBDD systems.

In order to describe transport and adsorption behaviors of the dynamic system, a modified Darcy law is employed within the desiccant porous media, and the adsorption characteristics of the M. S. Gel adsorbent (based on an independent gravimetric experiment) are directly incorporated into the mass conservation equation. And it is coupled with the moisture adsorption rate to consider the latent heat of phase transition due to the moisture condensation and heat loss during the dehumidification process to capture temperature variations.

2. Mathematical model

2.1. System description

The MFBDD system described in Part I is schematically illustrated in Fig. 1. According to the experimental system, humid air was supplied into parallel flow channels (between the M. S. Gel desiccant beds) through an inlet chamber for the dehumidification process. Additionally, M. S. Gel beads (manufactured by AGC Si-Tech Co., Ltd., Japan) were supported by highly thermal conductive metal frames on which a coarse mesh structure allowed free penetration of moisture into the desiccant adsorbent. The humidity and temperature of the dehumidified air were measured at the outlet of the MFBDD. In the model, transient humidity and temperature variations around an M. S. Gel desiccant bed were considered between two air flow channels by employing a 2D Cartesian coordinate (x, y) system (in which boundary effects in the z-direction are neglected).

2.2. Governing equations

The transport behavior of the air flow vector $\mathbf{v}$ (corresponding to the Darcy velocity vector in the M. S. Gel bed that denotes the product of porosity ε and the local average velocity vector $\mathbf{v}_{local}$, *i.e.*, $\mathbf{v} = \varepsilon\mathbf{v}_{local}$ [12]), specific humidity X, and temperature T are derived by solving the conservation equations of momentum, mass, and energy. The process air is considered as an incompressible fluid that satisfies a steady-state continuity equation as follows:

$$\nabla \cdot \mathbf{v} = 0 \tag{1}$$

For the momentum balance of the air flow, the Navier-Stokes equation is employed in the air flow channel (Eq. (2a)). A modified Navier-Stokes equation based on an extended Darcy-Brinkman

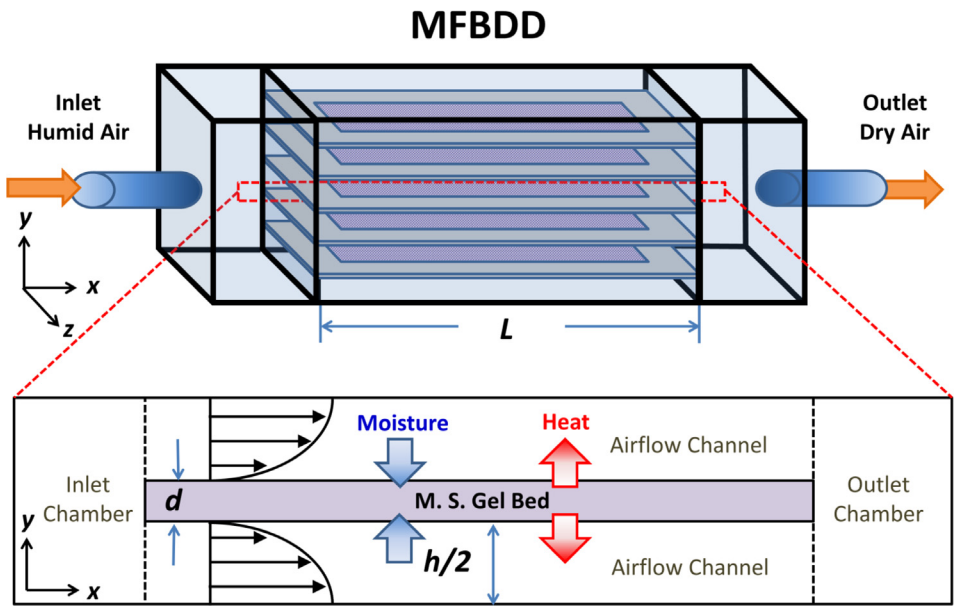

Fig. 1. A schematic diagram of the MFBDD simulation domain highlighted by the red dashed rectangle. 2 D Cartesian coordinates are employed (x, y) where $L = 20$ cm, $d = 1$ mm, and $h = 4$ mm correspond to the length of the M. S. Gel bed, M. S. Gel bed thickness, and air flow channel size, respectively. (For interpretation of the references to color in this figure legend, the reader is referred to the web version of this article.)

equation [13,14] (Eq. (2b)) is employed such that an additional friction force term resulting from the presence of the M. S. Gel beads in the desiccant bed is considered as follows:

$$\rho\left(\frac{\partial \mathbf{v}}{\partial t} + \nabla \cdot \mathbf{vv}\right) = -\nabla P + \mu \nabla^2 \mathbf{v} \tag{2a}$$

$$\rho\left(\frac{1}{\varepsilon}\frac{\partial \mathbf{v}}{\partial t} + \frac{\nabla \cdot \mathbf{vv}}{\varepsilon^2}\right) = -\nabla P + \frac{\mu}{\varepsilon}\nabla^2 \mathbf{v} - \frac{\mu}{K}\mathbf{v} \tag{2b}$$

In these expressions, t denotes the time, $\rho = 1.225$ kg m^{-3} denotes the density of air [15], P denotes the pressure, $\mu = 1.983 \times 10^{-5}$ Pa s denotes the viscosity of air [15], $K = \frac{d_p^2 \varphi^2 \varepsilon^3}{180(1-\varepsilon)^2}$ denotes the permeability of the M. S. Gel bed [16] (in which $d_p = 100$ μm denotes the average M. S. Gel bead diameter, the sphericity $\phi = 1$ for spherical particles, and $\varepsilon = 0.3$ denotes the porosity of the M. S. Gel bed). It should be noted that $\frac{\partial \mathbf{v}}{\partial t}$ vanishes as the incompressible fluid assumption is applied rendering a steady-state behavior of the air flow.

With respect to the mass conservation of moisture in the air flow channels, the variation in X is subject to convection (*i.e.*, diffusion and advection) as described in Eq. (3a). Conversely, within the M. S. Gel bed, the adsorption phenomenon is substantial to the humidity variation (Eq. (3b)) as follows:

$$\frac{\partial X}{\partial t} + \mathbf{v} \cdot \nabla X = D\nabla^2 X \tag{3a}$$

$$\frac{\partial X}{\partial t} + \frac{\mathbf{v}}{\varepsilon} \cdot \nabla X = D\nabla^2 X - \frac{\rho_{\text{M. S. Gel}}}{\rho}\frac{(1-\varepsilon)}{\varepsilon}\frac{\partial M}{\partial t} \tag{3b}$$

where $D = 2.82 \times 10^{-5}$ m^2 s^{-1} denotes the water diffusivity in the air [15], $\rho_{\text{M. S. Gel}} = 1.1 \times 10^3$ kg m^{-3} denotes the density of the M. S. Gel, and M denotes the amount of water adsorbed in the M. S. Gel. The adsorption rate $M' = \frac{\partial M}{\partial t}$ of the desiccant layer is obtained by the Linear Driving Force (LDF) model [17] as follows:

$$M' = k_{\text{ads}}(M_{\text{eq}} - M) \tag{4}$$

where $k_{\text{ads}} = 5 \times 10^{-3}$ s^{-1} denotes the adsorption rate constant. The adsorbed water at equilibrium M_{eq} is estimated by fitting experimental adsorption characteristics of the M. S. Gel at room temperature as shown in Fig. 2. The sigmoid-shape adsorption characteristic of the M. S. Gel are described by employing a modified Langmuir-Sips adsorption model [18] as follows:

$$M_{\text{eq}} = a\left(\frac{b_1\varphi}{1+b_1\varphi} + \frac{b_2\varphi^n}{1+b_2\varphi^n}\right) \tag{5}$$

where $a = 0.39$ kg kg^{-1}, $b_1 = 2 \times 10^{-11}$, $b_2 = 2 \times 10^{-2}$, and $n = 6$ are constant parameters and $\phi = p_v/p_{\text{sat}} \times 100$ (%) denotes the relative humidity in percentage where p_v denotes the partial vapor pressure and p_{sat} denotes the saturation vapor pressure. For simplicity, the ideal gas law is employed for p_v as follows:

$$p_v = \frac{X\rho RT}{M_w} \tag{6}$$

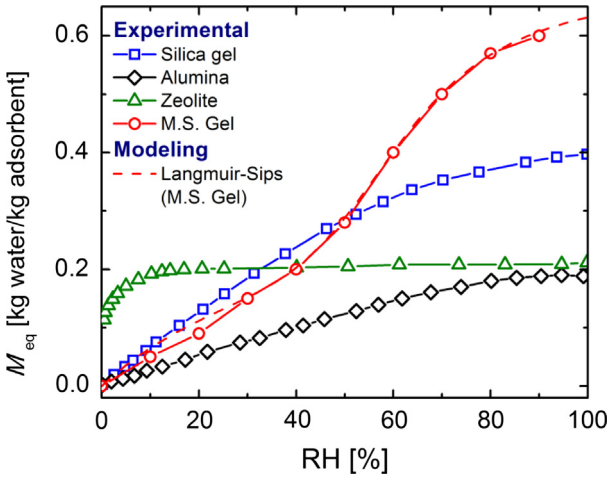

Fig. 2. Variations of the adsorbed water at equilibrium M_{eq} (at room temperature) for different relative humidity (RH) levels for various adsorbents [20,21]. The red dashed curve denotes the theoretical fitting of the M. S. Gel isotherm by the modified Langmuir-Sips theory (Eq. (5)). (For interpretation of the references to color in this figure legend, the reader is referred to the web version of this article.)

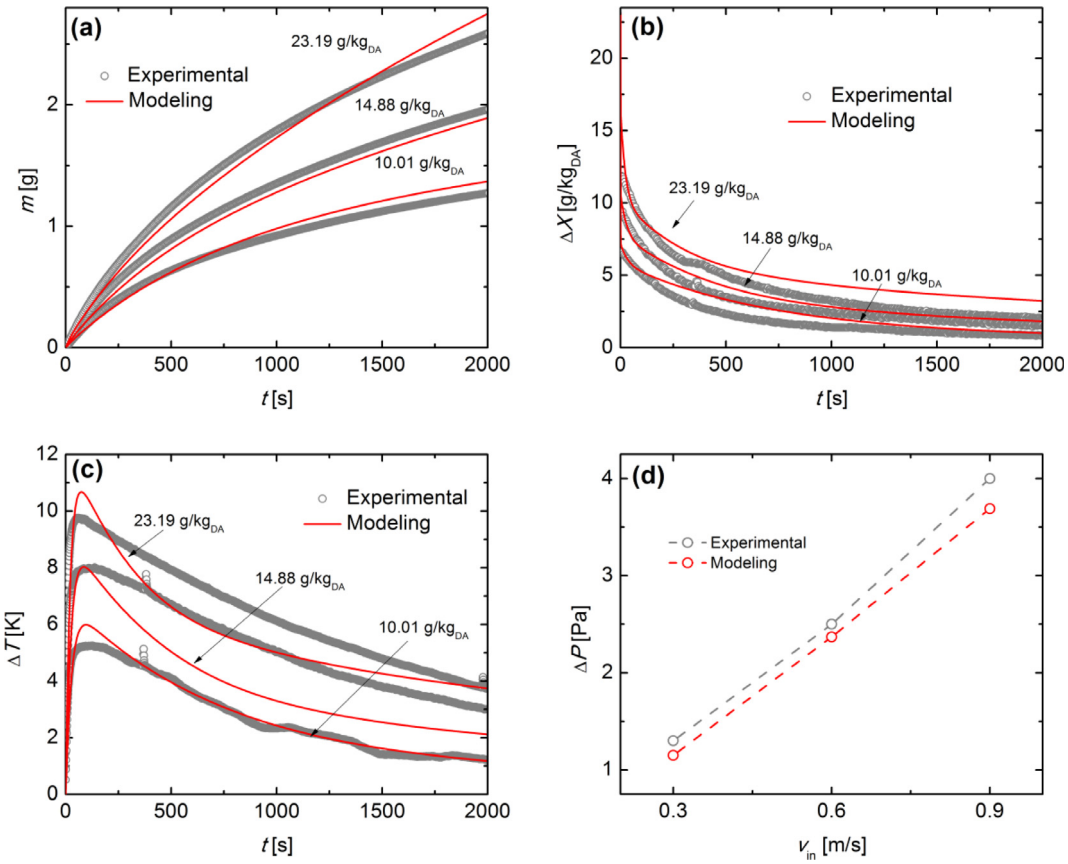

Fig. 3. Transient responses of the (a) adsorbed water m, (b) dehumidification capacity ΔX, and (c) temperature increase ΔT at different levels of inlet humidity X_{in} at v_{in} = 0.9 m/s, and (d) variation in the pressure drop ΔP for different inlet velocity v_{in} when comparing the experimental (gray) and theoretical (red) results. (For interpretation of the references to color in this figure legend, the reader is referred to the web version of this article.)

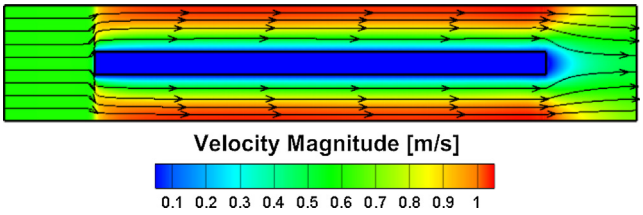

Fig. 4. Air velocity magnitude and flow streamlines at v_{in} = 0.6 m/s (the scale in the horizontal direction is shrunk by 10 times for visualization purposes).

where $R = 8.3145\ \mathrm{J\ mol^{-1}\ K^{-1}}$ denotes the ideal gas constant, and $M_w = 18.015\ \mathrm{g\ mol^{-1}}$ denotes the molar mass of water [15]. The saturation vapor pressure p_{sat} is described by the Tetens equation [19] as follows:

$$p_{sat} = 610.78 \exp\left(\frac{17.27(T - 273.15)}{T - 35.85}\right) \tag{7}$$

As shown in Fig. 2, the M. S. Gel possesses a higher adsorption capacity when compared with that of typical silica gel, alumina, or zeolite [20,21]. Additionally, its unique sigmoid-shape adsorption characteristic renders it competitive for air-conditioning applications. It is also more favorable for the regeneration process, and this allows the removal of moisture at a relatively humid condition.

With respect to heat transfer, the classical heat transport equation for air flows is used within air flow channels (Eq. (8a)). Two additional factors (including a heat source and heat loss term) are considered within the M. S. Gel bed (Eq. (8b)) such that (i) the latent heat is generated during the adsorption process and (ii) the highly thermal conductive metal frame enables considerable heat loss to the surroundings.

$$\frac{\partial T}{\partial t} + \mathbf{v} \cdot \nabla T = \alpha_{air} \nabla^2 T \tag{8a}$$

$$\frac{\partial T}{\partial t} + \frac{\rho C_p}{\rho_{bed} C_{p,bed}} \mathbf{v} \cdot \nabla T = \alpha_{bed} \nabla^2 T + \frac{h_{ads} \rho_{M.\ S.\ Gel} (1 - \varepsilon)}{\rho_{bed} C_{p,bed}} \frac{\partial M}{\partial t} - \frac{h_{loss}}{\rho_{bed} C_{p,bed}} (T - T_0) \tag{8b}$$

In these expressions, $\alpha_{air} = 1.9 \times 10^{-5}\ \mathrm{m^2\ s^{-1}}$ denotes the thermal diffusivity of air [15] and $\alpha_{bed} = \frac{k_{bed}}{\rho_{bed} C_{p,bed}}$ denotes the thermal diffusivity of the M. S. Gel bed based on silica where the net thermal conductivity of the bed $k_{bed} = \varepsilon k + (1 - \varepsilon) k_{M.\ S.Gel}$ [22] and the product of the density and the specific heat capacity of the bed $\rho_{bed} C_{p,\ bed} = \varepsilon \rho C_p + (1 - \varepsilon) \rho_{M.\ S.\ Gel} C_{p,\ M.\ S.\ Gel}$ are derived from the contribution of the M. S. Gel and the air averaged by ε. The thermal conductivity of air $k = \alpha_{air} \rho C_p$ in which the specific heat capacity of air $C_p = 1.03 \times 10^3\ \mathrm{J\ kg^{-1}\ K^{-1}}$ [15] whereas the thermal conductivity of the M. S. Gel. $k_{M.\ S.\ Gel} = \alpha_{M.\ S.\ Gel} \rho_{M.\ S.Gel} C_{p,\ M.\ S.\ Gel}$ such that the thermal diffusivity of the M. S. Gel $\alpha_{M.\ S.\ Gel} = 8.3 \times 10^{-7}\ \mathrm{m^2\ s^{-1}}$ and the specific heat capacity of the M. S. Gel $C_{p,M.\ S.\ Gel} = 9.21 \times 10^2\ \mathrm{J\ kg^{-1}\ K^{-1}}$. Furthermore, $h_{ads} = 2.26 \times 10^6\ \mathrm{J\ kg^{-1}}$ denotes the latent heat of water adsorption [15], $h_{loss} = 1.06 \times 10^4\ \mathrm{W\ m^{-3}\ K^{-1}}$ denotes the heat loss coefficient, and $T_0 = 300$ K is the surrounding room temperature.

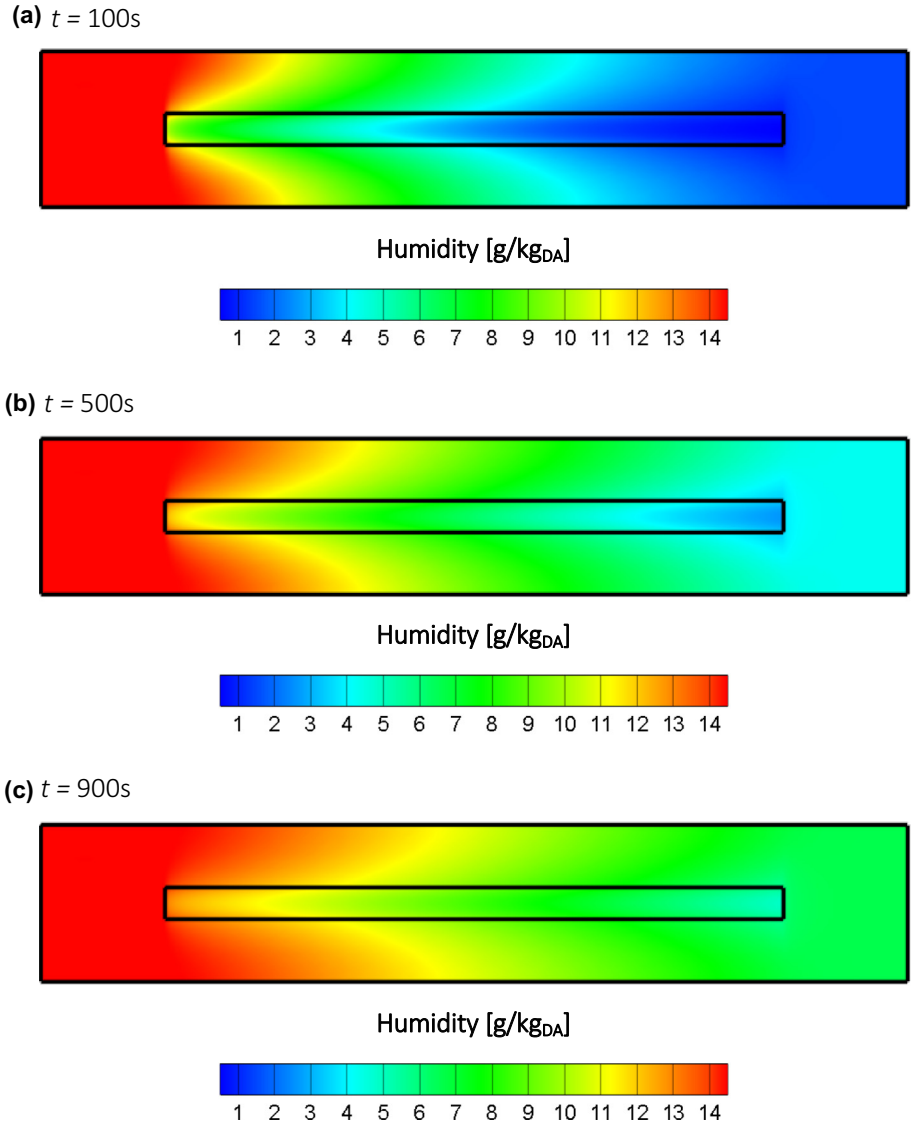

Fig. 5. Transient spatial variation of the humidity X within the MFBDD at X_{in} = 14.88 g/kg$_{DA}$, v_{in} = 0.3 m/s and (a) t = 100 s, (b) t = 500 s, and (c) t = 900 s (the scale in the horizontal direction is shrunk by 10 times for visualization purposes).

2.3. Initial and boundary conditions

In the experimental system in Part I, the MFBDD was initially filled with stationary nitrogen gas at room temperature such that the humidity approached zero. According to the setup, in the model, it is assumed that at $t = 0$, the air is stagnant and completely dry and that temperature reaches equilibrium with respect to the surrounding temperature as follows:

$$\mathbf{v} = \mathbf{0}, \quad X = 0 \quad \text{and} \quad T = T_0 \tag{9}$$

On the boundaries, it is assumed that the velocity, inlet specific humidity X_{in}, and inlet air temperature $T_{in} = T_0 = 300$ K are uniform in the y-direction at the MFBDD inlet boundary (the end of the inlet chamber). Similarly, with respect to the outlet of the MFBDD, it is assumed that the air flow is fully developed and that the outlet specific humidity X_{out} and the outlet air temperature T_{out} are uniform in the flow (horizontal) direction. Symmetry conditions are applied to the air flow channel centerlines implying that there is no variation in the y-direction for each variable.

At the interfaces of the M. S. Gel bed and air flow channels, it is assumed that the air velocity, air flux, pressure, pressure gradient, humidity, moisture flux, and diffusive heat transfer are continuous (Eqs. (10a)–(10d)) [23]. Additionally, the convective heat flux to the air flow channel is equivalent to diffusive heat from the M. S. Gel bed (Eq. (10e)) [24]. This leads to the following boundary equations:

$$\mathbf{v}|_{\text{flow channel}} = \mathbf{v}|_{\text{bed}}, \quad \mathbf{n}\cdot\nabla\mathbf{v}|_{\text{flow channel}} = \mathbf{n}\cdot\nabla\mathbf{v}|_{\text{bed}} \tag{10a}$$

$$P|_{\text{flow channel}} = P|_{\text{bed}}, \quad \mathbf{n}\cdot\nabla P|_{\text{flow channel}} = \mathbf{n}\cdot\nabla P|_{\text{bed}} \tag{10b}$$

$$X|_{\text{flow channel}} = X|_{\text{bed}}, \quad \mathbf{n}\cdot\nabla X|_{\text{flow channel}} = \mathbf{n}\cdot(\varepsilon\nabla X)|_{\text{bed}} \tag{10c}$$

$$\mathbf{n}\cdot(k\nabla T)|_{\text{flow channel}} = \mathbf{n}\cdot(k_{\text{bed}}\nabla T)|_{\text{bed}} \tag{10d}$$

$$h_c(T|_{\text{bed}} - \bar{T}) = -\mathbf{n}\cdot(k_{\text{bed}}\nabla T)|_{\text{bed}} \tag{10e}$$

where $\mathbf{n}$ denotes the normal vector on the M. S. Gel layer and the air flow channel boundary directing outward to the air flow channel, h_c = 7.5 W m^{-2} K^{-1} denotes the convective heat transfer coefficient between the M. S. Gel bed and the air in the air flow channels and flow average temperature [25] $\bar{T} = \langle v_x T\rangle / \langle v_x\rangle$ where the quantities $\langle v_x T\rangle$ and $\langle v_x\rangle$ correspond to the arithmetic averages of the product

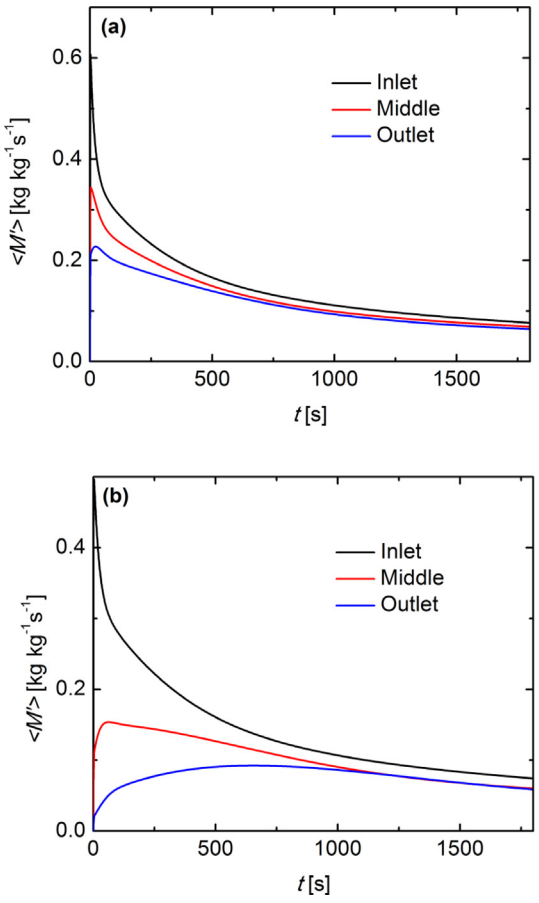

Fig. 6. Transient response of the average adsorption rate ⟨M′⟩ at different positions of the M. S. Gel bed at X_{in} = 14.88 g/kg$_{DA}$ and (a) v_{in} = 0.3 m/s and (b) v_{in} = 0.9 m/s.

of the air velocity in the x-component v_x and temperature and v_x across the air flow channel in the y-direction, respectively. On the M. S. Gel. bed boundaries facing the inlet and outlet chambers, the following equations hold: $\bar{T} = T_{in}$ and T_{out}, respectively.

2.4. Output parameters

The performance of the M. S. Gel dehumidifier is evaluated based on the total adsorbed water within the M. S. Gel dehumidifier m, dehumidification capacity ΔX, temperature increase ΔT, and pressure drop ΔP:

$$m = N \iint W \rho M (1-\varepsilon) dA \tag{11a}$$

$$\Delta X = X_{in} - X_{out} \tag{11b}$$

$$\Delta T = T_{out} - T_{in} \tag{11c}$$

$$\Delta P = P_{out} - P_{in} \tag{11d}$$

where N = 5 denotes the number of M. S. Gel beds in the MFBDD, W = 1 cm denotes the width of the MFBDD, A denotes the simulation domain of the M. S. Gel bed, and P_{out} and P_{in} denote the pressure at the inlet and outlet of the MFBDD, respectively. Based on the experimental measurements of the local transient variations, the arithmetic averages of adsorption rate $\langle M' \rangle$ and temperature $\langle T \rangle$ are output in the y-direction at x = 1 cm, 10 cm, and 19 cm (that are referred as to the inlet, middle, and outlet, respectively, as shown in Figs. 6 and 8) both in the air flow channel and the M. S. Gel bed (where x = 0 cm is anchored at the junction of the inlet chamber and the air flow channels).

The present boundary problem is solved by using an implicit finite volume framework [15]. The typical cell number used by the structured computational mesh corresponds to 30,321. The time difference Δt = 1 s between each time step is adopted such that the sensitivity test shows an error percentage of ΔX between the results of Δt = 0.5 and 1 s is lower than 0.1%.

3. Results and discussion

3.1. Verification of the theoretical model

First, the constructed model is verified by comparing the theoretical predictions with the experimental observations reported in Part I. As shown in Fig. 3, the theoretical estimates of the momentum (pressure drop), mass (humidity), and heat (temperature) transfer behaviors of the MFBDD indicate close agreement with the experimental measurements.

As shown in Fig. 3a and b, m and ΔX increase at a higher X_{in} as expected. Initially, ΔX decreases steeply due to a rapid accumulation of water into the M. S. Gel bed, and thus a decrease in the adsorption rate. As shown in Fig. 3a, the increase in m evidently becomes gradually slower, and this implies the decrease in moisture removal ability due to partial saturation of a desiccant bed. When the M. S. Gel bed becomes completely saturated, m becomes time independent, and ΔX drops to zero indicating the termination of the adsorption process.

Furthermore, ΔT is a response to the latent heat released from the adsorption process, and thus it is directly affected by the adsorption behavior as described in Eq. (8b). As shown in Fig. 3c, ΔT initially soars owing to a high adsorption rate. Additionally, the reduction in the adsorption rate is accompanied by a gradual decease in ΔT after experiencing a maximum value. On the other hand, it is worth noting that ΔP of the MFBDD only corresponds to 4 Pa even at a high inlet flow velocity v_{in}=0.9 m/s (the equivalent flow rate = 16 L/min).

3.2. Momentum transfer in the MFBDD

In the following sections, the transport phenomena of the results in Fig. 3 are analyzed with local resolution from the simulations. A typical air flow velocity profile is demonstrated in Fig. 4. The closely packed M. S. Gel beads inside the bed cause the air flow to experience a large friction force in the M. S. Gel bed. Consequently, the enclosed air is merely immobile, and this makes the air velocity profiles similar to that in gas-impermeable slit channels. When compared with conventional honeycomb structure desiccant rotary wheels, the present multilayered structure possesses a significantly lower pressure drop across the unit. Thus, it is favorable for large air-conditioning facilities where the power consumption of fans contributes a considerable proportion to the overall energy usage.

3.3. Transient behavior of moisture transfer in the MFBDD

When wet air is supplied into the MFBDD, the moisture carried by the stream is spontaneously adsorbed into the M. S. Gel bed. Therefore, as shown in Fig. 5, a humidity gradient is generated in the flow normal direction rendering X on the air channel centerline higher than that in the vicinity of the desiccant bed. As time elapses, this humidity gradient gradually decreases (when compared to that between Fig. 5a and c). Furthermore, the outlet humidity increases, and thus indicates the reduction of the moisture removal efficiency due to the partial saturation of the M. S. Gel bed.

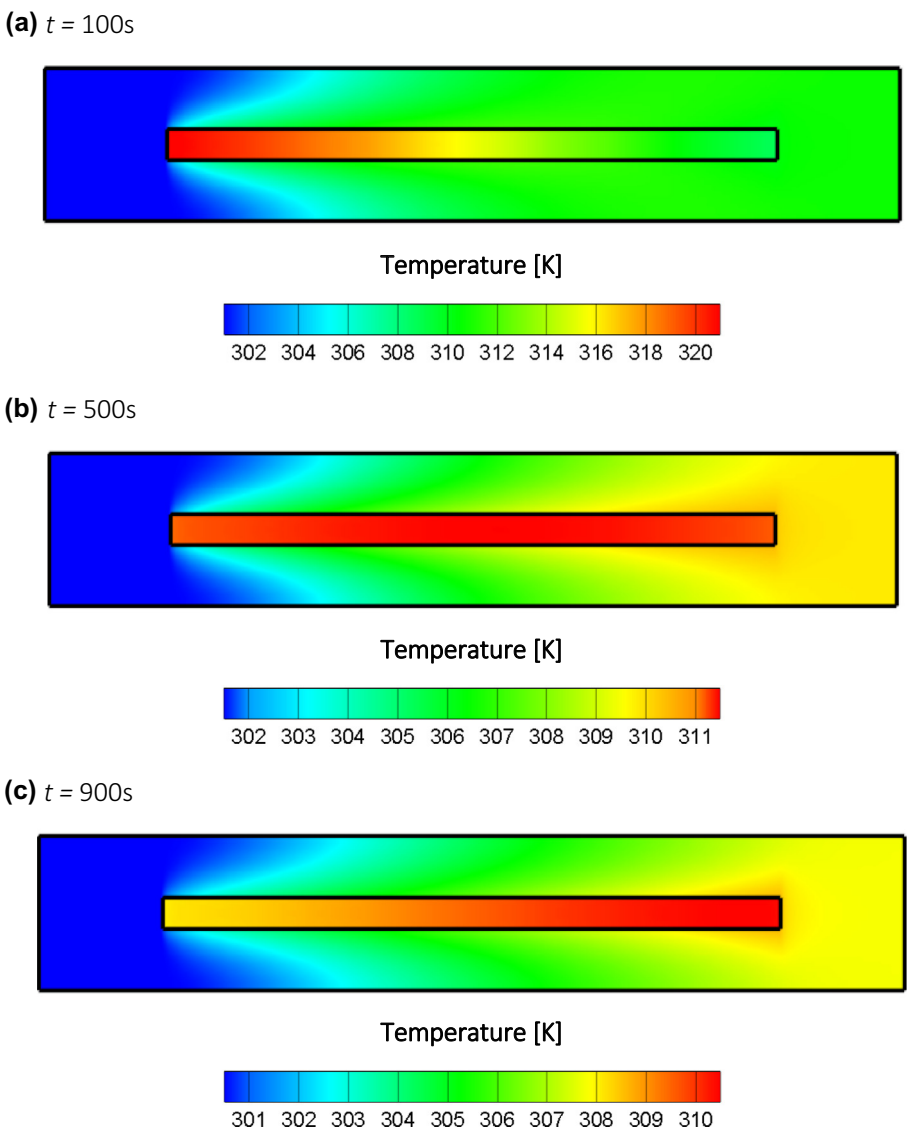

Fig. 7. Transient spatial variation of the temperature T within the MFBDD at X_{in} = 14.88 g/kg$_{DA}$, v_{in} = 0.3 m/s, and (a) t = 100 s, (b) t = 500 s, and (c) t = 900 s (the scale in the horizontal direction is shrunk by 10 times for visualization purposes).

Fig. 6 shows the transient behavior of average adsorption rate $\langle M' \rangle$ at different locations of the M. S. Gel bed. Moisture adsorption into the M. S. Gel bed is driven by diffusion in air flow channels (in which the flux is proportional to the vertical humidity gradient), and thus $\langle M' \rangle$ at the inlet exceeds that at the outlet due to a X humidity of the inlet air. The initial spatial difference of $\langle M' \rangle$ is evident although it becomes marginal when the M. S. Gel bed is saturated. It should be noted that this spatial variation of $\langle M' \rangle$ is susceptible to the air velocity. At a high air velocity (v_{in} = 0.9 m/s in Fig. 6a), the spatial difference is smaller than that at a lower air velocity (v_{in} = 0.3 m/s in Fig. 6b). In extreme cases in which $v_{in} \to \infty$ or $v_{in} \to 0$, the difference vanishes for high–speed cases while $\langle M' \rangle$ at the outlet approaches zero for the latter case since the supplied moisture is completely adsorbed around the inlet of the M. S. Gel bed.

3.4. Transient behavior of heat transfer in the MFBDD

During the adsorption of moisture into the M. S. Gel, phase transition latent heat is simultaneously released increasing the temperature of the bed and surrounding air. Therefore, while X gradually reduces toward the downstream, T is increased in the air flow channel as shown in Fig. 7. Interestingly, in contrast to the air flow channel in which the highest T occurs at the outlet (as shown in Fig. 8b and d) throughout the adsorption process, the maximum T within the M. S. Gel bed relocates from the inlet end toward the outlet end (as shown in Fig. 8a and c). The released heat of phase transition during the adsorption at the inlet of the M. S. Gel bed is proportional to $\langle M' \rangle$ (as described in Eq. (8b)) and remains higher than that from the outlet (as evidenced by a higher $\langle M' \rangle$ at the inlet of the M. S. Gel bed through the whole adsorption process in Fig. 6). Therefore, this sole mechanism is insufficient to explain the unique phenomenon observed (both experimentally and theoretically). Accordingly, it is concluded that the translocation of the maximum temperature in the M. S. Gel bed is due to competition between the (i) supplied air temperature from the inlet (lowering T) and (ii) latent heat released (lifting T). At the beginning of the dehumidification process, the heat that contributed due to the adsorption rate is dominant and this makes T higher at the inlet of the M. S. Gel bed. As partial saturation of the M. S. Gel bed occurs, the decrease in the adsorption rate makes the former factor more crucial to the tem-

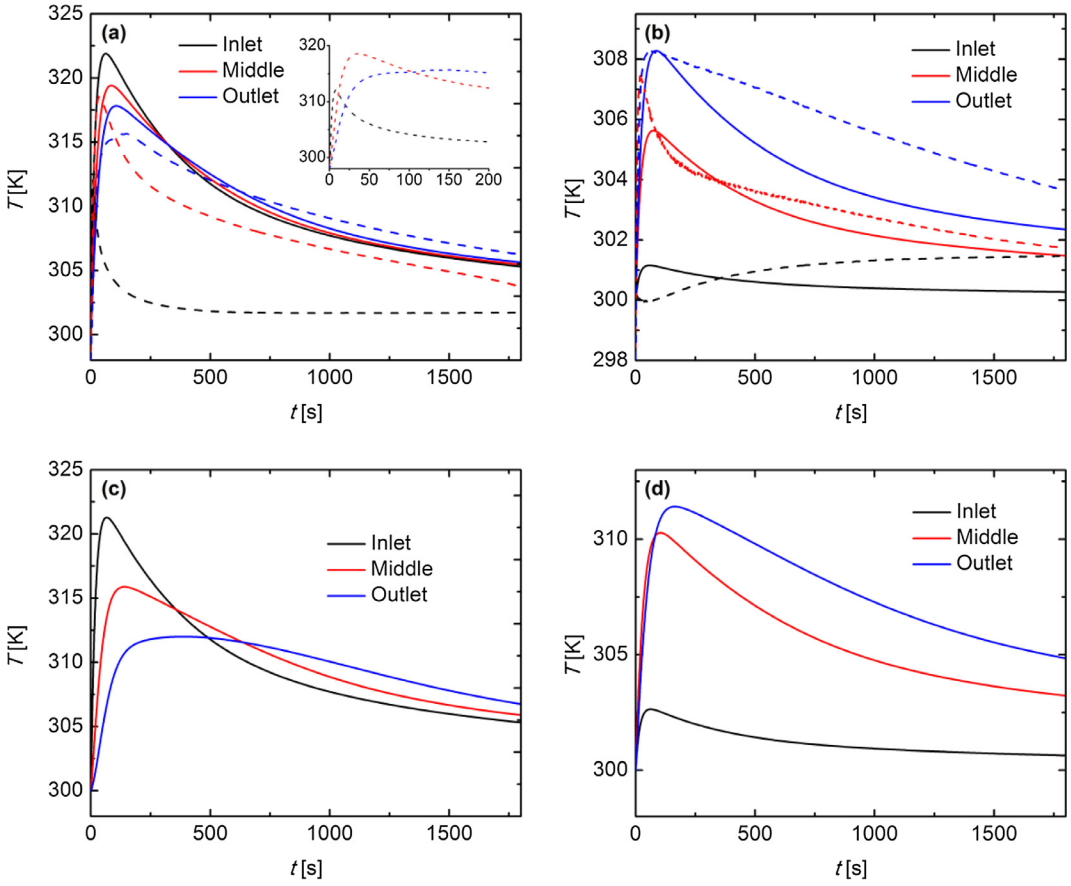

Fig. 8. Transient responses of the temperature T at different positions of the (a) M. S. Gel bed (inset zooms in the initial 200 s of the experimental results) and (b) air flow channel at v_{in} = 0.9 m/s; and v_{in} = 0.3 m/s of the (c) M. S. Gel bed and (d) air flow channel. The solid curves are theoretical predictions at X_{in} = 14.88 g/kg$_{DA}$ and the dashed curves are experimental results at a similar inlet humidity level X_{in} = 14.2–14.8 g/kg$_{DA}$.

perature distribution of the M. S. Gel bed, and hence the peak T shifts toward the outlet end.

It is found that the transient ⟨T⟩ variation is significantly influenced by the speed of the process air. Although a higher v_{in} also enhances the adsorption rate (as shown in Fig. 6), the relocation speed of the peak T increases with increases in v_{in} (as shown in Fig. 8a and c). In Fig. 8a and b, the experimental results were compared with theoretical estimates at similar conditions. The results indicate that the experimental peak temperature shift was even faster than the theoretical predictions. For instance, the peak shifted to the outlet end in 2 min in the experiment while it takes about twice as long in the simulation at v_{in} = 0.9 m/s. This could be because the heat transfer behavior at the M. S. Gel and the air flow channel interface is more complicated than the simple model that was applied to Eq. (10e) in which the heat transfer coefficient h_c is assumed as constant for all conditions. However, in practice, h_c is influenced by the air flow velocity and end effects [25]. However, the results of the simulation show that despite the simplified interfacial heat transfer model, a qualitative agreement of the behavior is achieved.

4. Conclusions

In summary, a comprehensive 2D computational model has been established by using the momentum, mass, and energy conservation principles to investigate transport, adsorption, and thermal phenomena within a MFBDD. The constructed model has been verified by comparing theoretical predictions with the experimental measurements in Part I such that a quantitative agreement was achieved between these results with respect to dehumidification capacity, amount of adsorbed water, temperature increase, and pressure drop.

Due to its multilayered structure, the MFBDD demonstrates a low pressure drop characteristic (<10 Pa) that is superior to conventional desiccant rotary wheels. The spatial variations of transient moisture and heat transfer behavior were investigated in the MFBDD via the established model. The adsorption rate reaches its highest value at the inlet end of the M. S. Gel bed and gradually decreases toward the outlet end. This adsorption rate difference between two ends gradually shrinks with time and it is smaller for an increase in the air flow velocity. The air temperature inside the air flow channel increases toward the outlet during the adsorption. Conversely, the peak temperature of the M. S. Gel bed shifts from the inlet end toward the outlet end due to the competition between the lower inlet temperature and higher latent heat released at the inlet end of the M. S. Gel bed. The speed of this maximum temperature translocation increases with increases in air flow velocity.

The study has investigated a rigorous model that reproduces experimental observations and provides locally transient responses of heat and mass transfer in the dehumidifier, which constitutes a promising tool facilitating the development of MFBDD for high performance desiccant-based air-conditioning systems.

Acknowledgements

This work was supported by Asahi Glass Co. Ltd., Japan and the Japan Science and Technology Agency (JST-CREST) program "Phase Interface Science for Highly Efficient Energy Utilization."

References

[1] J.A. Shamim, W.-L. Hsu, K. Kitaoka, S. Paul, H. Daiguji, Design and performance evaluation of a multilayer fixed-bed binder-free desiccant dehumidifier for hybrid air-conditioning system: Part I – Experimental, Int. J. Heat Mass Transfer 116 (2018) 1361–1369.

[2] T.S. Ge, Y. Li, R.Z. Wang, Y.J. Dai, A review of the mathematical models for predicting rotary desiccant wheel, Renew. Sustain. Energy Rev. 12 (2008) 1485–1528.

[3] S. De Antonellis, C.M. Joppolo, L. Molinaroli, Simulation, performance analysis and optimization of desiccant wheels, Energy Build. 42 (2010) 1386–1393.

[4] M.A. Mandegari, H. Pahlavanzadeh, A study on the optimization of an air dehumidification desiccant system, J. Therm. Sci. Eng. Appl. 5 (2013) 041002.

[5] S. Yamaguchi, K. Saito, Numerical and experimental performance analysis of rotary desiccant wheels, Int. J. Heat Mass Transf. 60 (2013) 51–60.

[6] D.Y. Lee, D.S. Kim, Analytical modeling of a desiccant wheel, Int. J. Refrig. 42 (2014) 97–111.

[7] T. Tsujiguchi, Y. Osaka, A. Kodama, Study on the miniaturization of the desiccant wheel by the optimization of designing/operation concept, J. Chem. Eng. Jpn. 47 (2014) 608–614.

[8] K.J. Chua, Heat and mass transfer of composite desiccants for energy efficient air dehumidification: modelling and experiment, Appl. Therm. Eng. 89 (2015) 703–716.

[9] N. Giannetti, A. Rocchetti, K. Saito, S. Yamaguchi, Entropy parameters for desiccant wheel design, Appl. Therm. Eng. 75 (2015) 826–838.

[10] M. Intini, M. Goldsworthy, S. White, C.M. Joppolo, Experimental analysis and numerical modelling of an AQSOA zeolite desiccant wheel, Appl. Therm. Eng. 80 (2015) 20–30.

[11] D. Cheng, E. Peters, J.A.M. Kuipers, Numerical modelling of flow and coupled mass and heat transfer in an adsorption process, Chem. Eng. Sci. 152 (2016) 413–425.

[12] S. Whitaker, Flow in porous media. I. A theoretical derivation of Darcy's law, Transp. Porous Media 1 (1986) 3–25.

[13] M.A. Hossain, M. Wilson, Natural convection flow in a fluid-saturated porous medium enclosed by non-isothermal walls with heat generation, Int. J. Therm. Sci. 41 (2002) 447–454.

[14] C.T. Hsu, P. Cheng, Thermal dispersion in a porous medium, Int. J. Heat Mass Transf. 33 (1990) 1587–1597.

[15] W.M. Haynes, CRC Handbook of Chemistry and Physics, 96th ed., CRC Press, 2015-2016.

[16] D.A. Nield, A. Bejan, Convection in Porous Media, second ed., Springer-Verlag, New York, 1992.

[17] S. Sircar, J.R. Hufton, Why does the linear driving force model for adsorption kinetics work ?, Adsorpt-J. Int. Adsorpt. Soc. 6 (2000) 137–147.

[18] J.W. Lee, W.G. Shim, H. Moon, Adsorption equilibrium and kinetics for capillary condensation of trichloroethylene on MCM-41 and MCM-48, Micropor. Mesopor. Mater. 73 (2004) 109–119.

[19] F.W. Murry, On the computation of saturation vapor pressure, J. Appl. Meteorol. 6 (1967) 203–204.

[20] X. Zheng, T.S. Ge, R.Z. Wang, Recent progress on desiccant materials for solid desiccant cooling systems, Energy 74 (2014) 280–294.

[21] R.T. Yang, Adsorbents: Fundamentals and Applications, John Wiley & Sons, 2003.

[22] M. Dehghan, Y. Rahmani, D.D. Ganji, S. Saedodin, M.S. Valipour, S. Rashidi, Convection-radiation heat transfer in solar heat exchangers filled with a porous medium: homotopy perturbation method versus numerical analysis, Renew. Energy 74 (2015) 448–455.

[23] J.A. Ochoatapia, S. Whitaker, Momentum transfer at the boundary between a porous medium and a homogeneous fluid. I. Theoretical development, Int. J. Heat Mass Transf. 38 (1995) 2635–2646.

[24] B. Alazmi, K. Vafai, Analysis of fluid flow and heat transfer interfacial conditions between a porous medium and a fluid layer, Int. J. Heat Mass Transf. 44 (2001) 1735–1749.

[25] B.B. Bird, W.E. Stewart, E.N. Lightfoot, Transport Phenomena, second ed., John Wiley & Sons, 2007.